

Effect of rough wall on drag, lift, and torque on an ellipsoidal particle in a linear shear flow

Atul Manikrao Bhagat, Partha Sarathi Goswami*

Chemical Engineering Department, Indian Institute of Technology Bombay, Mumbai - 400076 (India)

Abstract

The present study provides a detailed description of the forces on an ellipsoidal particle in the vicinity of the rough wall. Three-dimensional numerical simulations are performed using body-fitted mesh to estimate the drag, lift, and torque coefficients. A large number of simulations are conducted over a range of parameters such as shear Reynolds number ($10 \leq Re_s \leq 100$), orientation angle ($0^\circ \leq \theta \leq 180^\circ$), and wall-particle separation distance ($0.1 \leq \delta \leq 2.0$) to get a comprehensive description of variation of the above coefficients. Using the simulation results, we develop the correlations for the drag and lift coefficients to describe the effect of rough wall, inclination angles, and particle Reynolds numbers on the hydrodynamic coefficients. The proposed correlations can be used for two phase flow simulation using Eulerian-Lagrangian framework.

Keywords: Drag, lift, torque, non-spherical particle, rough wall, linear shear flow

1. Introduction

The flow of suspensions containing nonspherical particles is ubiquitous in natural, industrial, and biomedical processes. Industrial processes like, fluidization [1], pneumatic transport of solids [2, 3], processing in paper industry [4, 5, 6], and wastewater treatments [7] deal with the flow of nonspherical particles. Raw materials used in all the processes deviate a lot from the ideal spherical structure. Transport and deposition of nonspherical particles in biological flows are also important issues to be addressed [3]. Therefore, understanding the forces and dynamics of the nonspherical particles helps to design and develop these processes. Most of the earlier studies deal with the spherical particles [8, 9, 10] where symmetry plays an important role to simplify the problem unless the particles are placed near the solid surfaces. But, nonspherical particles

*Corresponding author. Tel.: +91 22-2576 7230; fax: +91 22-2572 6895
Email address: psg@iitb.ac.in (Partha Sarathi Goswami)

increase the degrees of freedom based on their orientation with respect to the ambient flows.

An attempt to describe the dynamics of a nonspherical particle in viscous flow initiated almost a century back with the phenomenal work by Jeffery and Filon [11]. They described the motion of an ellipsoid in the creeping flow limit. Brenner [12, 13, 14] investigated the forces on particles with arbitrary shape in the Stokes flow limit using analytical theory and provided the expression for drag and lift forces. Later, an expression for the lift force on a nonspherical particle in shear flow was derived by Harper and Chang [15] using asymptotic expansions. A comprehensive discussion on the dynamics of elongated particles for a wide range of flow is reported by Lin et al. [16].

A number of investigations that analysed the hydrodynamic forces on the particles placed near the wall at very low Reynolds number have been reported [17, 18, 19, 20, 21, 22, 23]. The boundary integral method was used to estimate the force and velocity of nonspherical particles in shear flow in the Stokes flow limit [17]. It was reported that the wall effect is very localized near the wall, and there is a decrease in the effect of wall on hydrodynamic forces and torque as the non-sphericity of the particle increases. A spectral boundary element method was used by Pozrikidis [18] to describe the motion of spheroidal particles for very low particle Reynolds number. A modification of the Jeffery orbit due to the presence of wall was reported by the author. Kim et al. [20] studied the dynamics of a cylindrical particle near a stationary wall in linear shear flow at different Stokes numbers. They have reported that there is an increase in drag with the aspect ratio of the particle. However, the torque is independent of wall-normal distance.

During the last decade, a number of notable works to provide correlations to calculate drag and lift are reported for finite Reynolds numbers [24, 25, 26, 27, 28, 29]. Majority of those are obtained through data fitting and satisfy the theoretical formulation at the limiting cases. Using the experimental data reported in the literature, Holzer and Sommerfeld [24] reported a correlation to calculate drag coefficient, which includes the effect of particle shape, orientation angle, and particle Reynolds number. Their correlation successfully predicts the drag coefficient with a maximum deviation of 14%. Immersed Boundary Method (IBM) was used by Zastawny et al. [25] to estimate drag and lift forces on the nonspherical particles. The parameters used in their correlations are exclusive functions of aspect ratio. Andersson and Jiang [30] also used IBM to analyse the forces on ellipsoid with a very high aspect ratio in uniform flow at very low Reynolds number. They outlined the challenges in computation at such a low Reynolds numbers for various inclination angles and computation domains. Ouchene et al. [31, 26] computed drag, lift, and torque coefficients for uniform flow over ellipsoidal particle at moderate Reynolds number using body-fitted mesh and presented the correlations. Sanjeevi and Padding [32] and Sanjeevi et al. [27] analyzed the drag on a nonspherical particle at different inclination angles in a uniform flow and for different Reynolds numbers. Forces on the spherical particle in the vicinity of a rough wall for linear shear flow have been estimated by Lee and Balachandar [8]. Frohlich et al. [28] have also

performed a number of simulations using the Cartesian cut cell method for an ellipsoid in an unbounded uniform flow. They have reported that beyond certain aspect ratio (> 3), the flow is not influenced much with the aspect ratio. Zarghami and Padding [22] examined the hydrodynamic forces and torque acting on a particle placed near the wall with 2D numerical simulations using Lattice Boltzmann method. A significant variation of forces based on wall separation and orientation angle was observed. The presence of a wall was found to change the directions of lift and torque acting on the particle [22]. Palmer and Smith [23] modeled the partially immersed finite body in viscous layers near a wall in a 2-dimensional scenario. Their study showed the oscillating motion of particles based on the center of mass of the particle. This motion of body directs the fluid displacement in between wall and particle, which results in non-linear pressure responses of a wall. All of these works were carried out either at Stokes flow regime or at a 2-D scenario. Very recently Fillingham et al. [29] developed correlations for the drag, lift, and torque coefficients on an ellipsoid particle placed on a smooth wall in a linear shear flow. They carried out a number of simulations at several combinations of parameters such as incident angle (in the plane perpendicular to the plane of shear), Reynolds number of flow, and aspect ratio of particle. The data from simulations were used to formulate the correlations, which reproduce the results for a spherical particle [10] as a limiting case. They have reported a maximum deviation of 16% as predicted by the correlation.

In the present study, we analyse the forces acting on an ellipsoidal particle in a linear shear flow. The particle is placed in the vicinity of a rough wall. 3D finite element method with body-fitted meshes is used for the simulations. The ellipsoidal particle is assumed to be fixed at a predefined distance away from the rough wall with an inclination angle. The objective is to estimate the forces acting on a particle at different distances from the rough wall and at various orientations with flow direction in the plane of shear. The effects of variation of the above parameters and the flow Reynolds number on the drag, lift, and torque coefficients acting on the particle are reported in detail. For all parameters investigated here, corresponding studies are carried out for the domain with a smooth wall. The results for the rough wall have been compared with the results for the smooth wall. Semi-empirical correlations are reported to predict the drag and lift coefficients for different inclination angles and a wide range of Reynolds numbers.

2. Numerical method

This section outlines the numerical technique used for the simulations. First, we describe the system configuration followed by the governing equations. Then, a validation study is presented for the flow conditions reported in the literature. Finally, an assessment for the flow development and finding particle location to obtain steady forces are presented.

A schematic of the domain, along with coordinate system used, is shown in Fig. 1. An ellipsoidal particle with semi-major axis a , semi-minor axis b (aspect

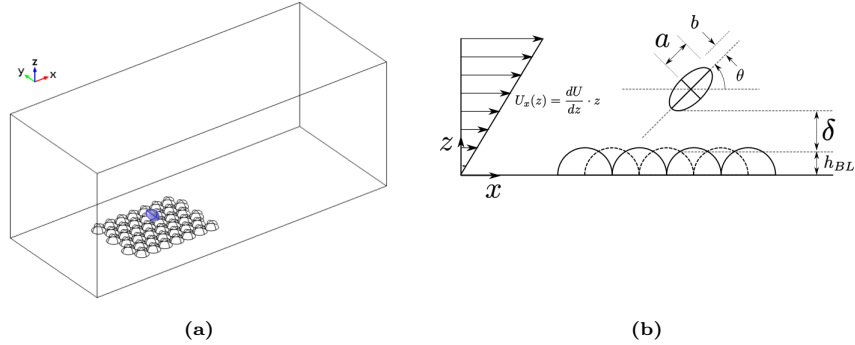


Fig. 1. (a) Domain for numerical analysis (3D) (b) Ellipsoid particle in domain

ratio $AR = a/b$), is placed at a location of L from the horizontal base wall. In the present study, all kinds of motion of ellipsoid such as rolling, tumbling, and linear movement are not considered; essentially forces on the stationary particle are analysed. The origin of a coordinate system is located on the base wall. A rough base plane is constructed using hemispherical particles of diameter d . These hemispheres are arranged in a triangular array fashion and in contiguity to generate a compact structure. The location of these hemispheres on the base plane is calculated using the method given by Lee and Balachandar [8] as,

$$\begin{aligned}
 x_{ij} &= \begin{cases} x_o + j & \text{if } i \text{ is odd} \\ x_o + (j - \frac{1}{2}) & \text{if } i \text{ is even} \end{cases} \\
 y_{ij} &= y_o + \sin\left(\frac{\pi}{3}\right)(i - 1) \\
 z_{ij} &= 0
 \end{aligned} \tag{1}$$

Here x , y , and z are scaled with equivalent diameter of particle d_p . Hemispheres are arranged in rows (i) and columns (j). The first row of hemispheres is kept at 5 particle diameters away from the entrance (at $x_0 = 5$). The value of y_o (≈ -2.165) is maintained such that there should be equal numbers of rows of hemispheres across ellipsoidal particle in channel cross-section.

Due to the presence of roughness on the wall, the effective clearance between the ellipsoid and the base plane is different as compared to a smooth wall. In case of the smooth wall, clearance (wall separation) is the distance from base plane to closest point on the ellipsoid in vertical direction. On the other hand, for rough wall, the minimum vertical distance changes with location of particle due to non-uniform surface. In that case, two different base levels are needed to be defined. First one is the actual wall base where the hemispheres are centered, and the other one is the bed height. Based on two-dimensional configuration the bed height is defined as minimum vertical distance between base level and lowest point on the ellipsoid, when it is seating on the bed. For the present configuration the bed height h_{BL} is taken to be $0.3165d_p$. Further, the clearance

of the ellipsoid from the bed height (δ) and orientation angle (θ) are the key parameters considered in the present study. δ is scaled with volume equivalent spherical particle diameter. The rotation of ellipsoid defined through orientation angle (θ), is about y -axis, and anticlockwise rotation is assumed to be positive.

A linear shear flow is considered to advance towards the rough surface with mean a velocity component in x -direction only and no flow in the span-wise direction. The velocity profile can be expressed as $U_x(z) = G_x z$ with $G_x = dU_x/dz$, a shear rate of approaching flow. Here, suffix x , represents inlet flow in x -direction. The shear Reynolds number based on the applied shear can be defined as,

$$Re_s = \frac{G_x d_p^2}{\nu}. \quad (2)$$

Here, d_p is related to major and minor axes of ellipsoid as $r_p = 2 \times (ab^2)^{1/3}$. The hydrodynamic coefficients for drag, lift, and torque based on the volume equivalent spherical diameter and ambient fluid velocity (U_x) at the center of mass location of ellipsoid ($z' = L$) are defined as

$$C_D = \frac{F_d}{\frac{1}{2}\rho U_x^2 \pi \frac{d_p^2}{4}}, C_L = \frac{F_L}{\frac{1}{2}\rho U_x^2 \pi \frac{d_p^2}{4}}, C_M = \frac{F_T}{\frac{1}{2}\rho U_x^2 \pi \frac{d_p^3}{8}}. \quad (3)$$

2.1. Governing equations

Flow of incompressible Newtonian fluid in the described domain is governed by the continuity and Navier-Stokes equations as,

$$\rho \left(\frac{\partial \mathbf{u}}{\partial t} + \mathbf{u} \cdot \nabla \mathbf{u} \right) - \nabla \cdot \boldsymbol{\sigma} = 0 \quad \text{on } \Omega(\mathbf{x}, t) \quad (4)$$

and

$$\nabla \mathbf{u} = 0 \quad \text{on } \Omega(\mathbf{x}, t). \quad (5)$$

Here, $\boldsymbol{\sigma}$ is a stress tensor, and is expressed as,

$$\boldsymbol{\sigma} = -p\mathbf{I} + \mathbf{T} \quad (6)$$

$$\mathbf{T} = 2\mu\boldsymbol{\varepsilon}(\mathbf{u}) \quad (7)$$

and $\boldsymbol{\varepsilon}(\mathbf{u})$, the deformation tensor can be expressed as,

$$\boldsymbol{\varepsilon}(\mathbf{u}) = \frac{1}{2} \left[(\nabla \mathbf{u}) + (\nabla \mathbf{u})^T \right]. \quad (8)$$

p and t are the pressure and time respectively. The simulations are done using COMSOL Multiphysics. The no-slip boundary condition is applied on the surface of ellipsoid and on the rough wall. Fully developed linear shear flow profile is imposed at the inlet. Free slip condition with no-flow across it, is set for the top wall. The domain is discretized using non-uniform tetrahedral grids. An

extremely fine grid size is imposed on the surface of rough wall and ellipsoid, in order to capture the flow gradient correctly. A large number of simulations have been carried out using different angles of inclination of the particle and the wall normal separation distances. Hydrodynamic forces on the particle are calculated and results obtained are discussed in the next section.

2.2. Validation

Before analyzing the results related to forces on an ellipsoid, the validation is conducted using the data from other simulations reported in the literature and with theoretical results, if available. The validations have been performed for two different cases. In the first case, the drag and the lift coefficients for ellipsoid (aspect ratio $AR = 2.5$) in uniform flow at low Reynolds number ($Re_p = 0.1$) is computed. The results have been compared with DNS results of Zastawny et al. [25], as shown in the Figs. 2a and 2b. The figures show a variation of the coefficients with angle of inclination. Drag and lift coefficients predicted by the present simulations show a good agreement with that predicted theoretically by Happel and Brenner [33]. There is an insignificant difference (about 0.3%) in drag coefficient as predicted by Zastawny et al. [25] using Immersed Boundary Method (IBM). Our results on lift coefficient, show a deviation of less than 5% from that predicted by Zastawny et al. [25] at an angle of $\theta = 45^\circ$. The

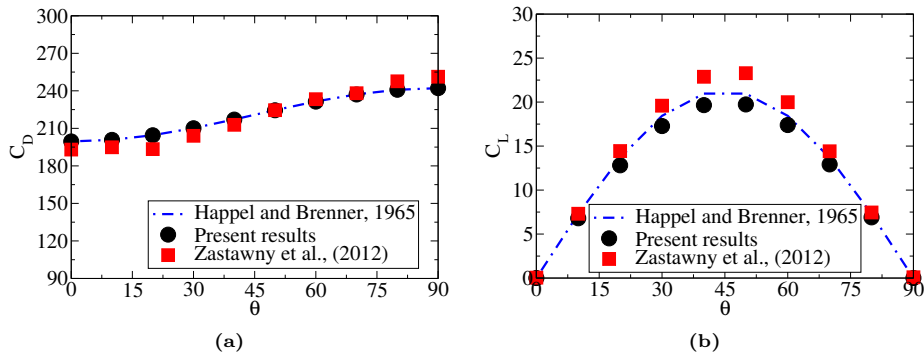


Fig. 2. Force coefficients for ellipsoid particle in uniform flow, compared with results of Zastawny et al. [25]

second set of validations is performed by analysing the flow over a spherical particle near the rough surface. The results (Fig. 3) are compared with Lee and Balachandar [8] who investigated hydrodynamic forces acting on spherical particle in an uniform shear flow over rough wall using IBM for a shear Reynolds number $Re_s \leq 100$. Figs. 3a and 3b show the drag and lift coefficients for particle at different location above the rough wall at $Re_s = 100$. It is observed that the results are in good agreement with the results of Lee and Balachandar [8]. A small difference is observed when the particle is placed very close to the wall. In any of the cases, maximum difference is always less than 5%. The results from the correlation by Zeng et al. [10] are plotted with similar conditions and found

to under predict the value. It is to be noted that results reported by Zeng et al. [10] are for the case of smooth wall.

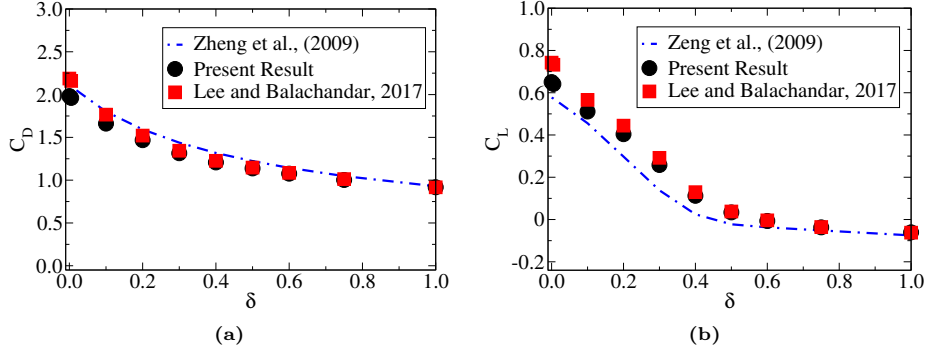


Fig. 3. Force coefficients for spherical particle in uniform shear flow, compared with results of Lee and Balachandar [8]

2.3. Flow development analysis

A fully resolved 3D simulations with body fitted fine mesh is computationally very much expensive. In the present study, the bottom wall is made rough using hemispheres of equivalent diameter of the ellipsoid. Such an arrangement also adds up to the overall computational cost. One of the major reason for this is the requirement of fine mesh on these hemispheres as well to capture the boundary layer on the particle. Therefore, to optimize the computational cost, only a small section of the bottom wall is made rough with an ordered arrangement of the hemispheres as shown in Fig. 1a. First, simulations are carried out for flow over rough wall in the absence of particle. The rough bed is constructed arranging hemisphere in 10 rows and 20 columns. The shear Reynolds number is varied between 10 to 100. The flow profile obtained from the simulations are plotted at different span-wise locations in domain. Figs. 4a to 4c show ambient flow profiles as a functions of wall normal direction (z) at different x' and y' locations over rough bed. It is observed that the flow remains developed for all the cases. Fig. 4a shows the velocity profile at $y' = 0.144$, which represents the deep cavity (along trough) in to the rough surface. Similarly Fig. 4b shows velocity profile at $y' = 0.433$ that is the top position (along crest) on surface of hemispheres. In both the Figs. 4a and 4b, the velocity profiles are shown at different stream-wise locations ($x' = 10, 11, 12, 13, 14$, and 15). The figures depict that the flow becomes developed after $x' = 14$, that is after 9th row of hemispheres. Further investigation are carried out at $x' = 15$ and $y' = 0.144, 0.722$, and -1.010 , which represent a deepest cavities along $y' = 0.144$ column. The corresponding profiles are shown in Fig. 4c. Here, velocity profiles for all the considered positions along y' are seen to be merged into a single line, give the confidence that the velocity is almost identical along that column of hemispheres around $x' = 15$. The next set of simulations is conducted to

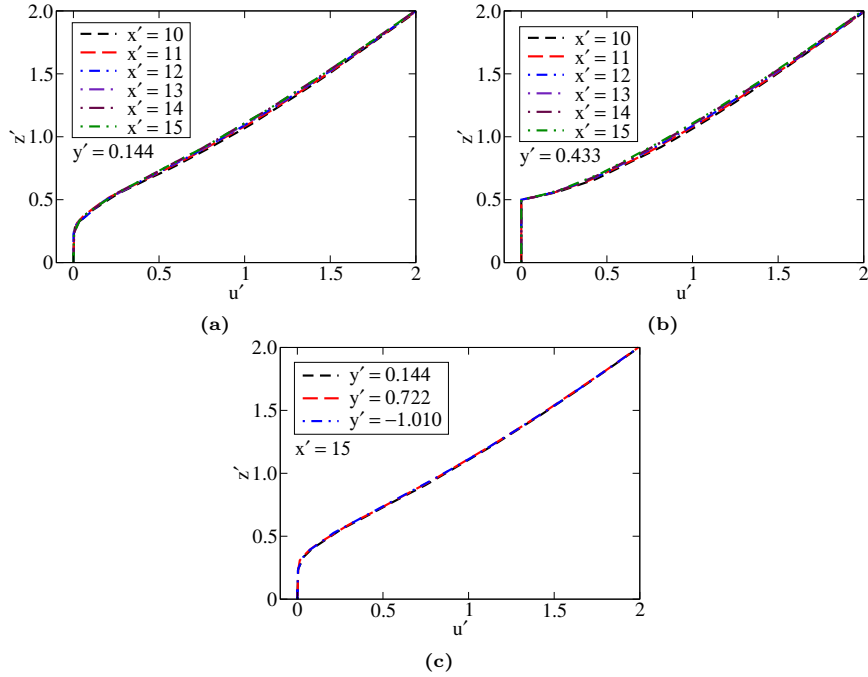


Fig. 4. Ambient velocity u variation with all normal direction z for $Re_s = 50$, at (a) $y' = 0.144$ and several x -locations, (b) $y' = 0.433$ and various x -locations, (c) $x' = 15$ and different y -locations

explore the location on the rough bed where the hydrodynamic forces on the particle are not be influenced by the edge effect of the rough bed. Three different cases are simulated based on the the Reynolds numbers (Re_s) 10, 50, and 100. Since presence of the wall affects the hydrodynamic forces acting on particle [10, 8, 22], it is important to carry out these test cases with particle positioned near the wall. Here we place the particle at $\delta = 0.1$ in z -direction, which presents the situation where the particle just touches the rough bed. The span-wise position, $y' = 0.144$ and the particle position is varied in x -direction ($x' = 10, 11, 12, 13, 14, 15, 16, \text{ and } 17$). The drag, lift, and torque coefficients are then calculated and are shown in Fig. 5. The figure shows that the variation of drag coefficient is only 0.5% for position higher than $x' = 15$. In case of the lift coefficient (Fig. 5b), the variation is small and it remains almost constant with an approximate change of 0.5% over entire range of the particle positions. Fig. 6 shows the variation of torque coefficient with particle position in stream-wise direction. An insignificant change is observed for particle position $x' < 15$ and for $x' > 15$ the coefficient appears to be constant having a maximum deviation of 0.2%. The above analysis confirms that a stream-wise distance $x' = 15$ or higher and a span-wise location $y' = 0.144$ can be considered to obtain hydrodynamic forces which are free of edge effects of rough bed.

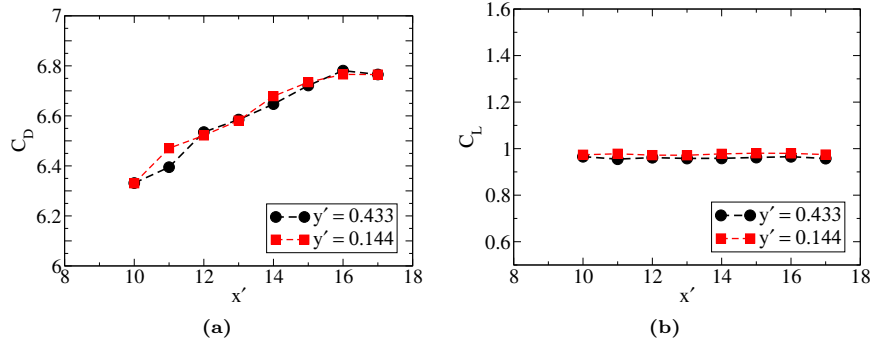


Fig. 5. (a) Drag and (b) lift coefficients variation over several x-position on rough bed ($\delta = 0.1$) for $y' = 0.144$, $Re_s = 10$ and $AR = 2$.

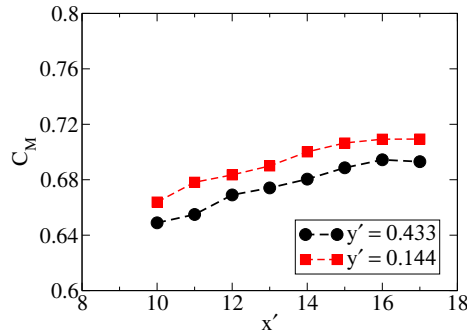


Fig. 6. Torque coefficient variation over several x-position on rough bed ($\delta = 0.1$) for $y' = 0.144$, $Re_s = 10$ and $AR = 2$.

2.4. Grid independence study

A proper grid resolution is a must to calculate accurate forces on the particle. Either the CFD results are to be validated with experiments to get an idea of proper resolution or in case of unavailability of the experimental data, grid-independent results are to be produced through different levels of grid refinements. There is no standard protocol yet to set-up the required grid resolution to analyse the flow over an object when it is placed near a wall with finite roughness [8]. Therefore, a grid independence study for the present work is of foremost importance. Use of an extremely fine mesh throughout the domain will also be computationally very expensive. Thus, an extremely fine mesh has been employed on the rough-surface using 3 layers of *boundary layer meshing*. The number of elements on the ellipsoid is then systematically varied in order to obtain a converge solution of the flow. The effect of variation of number of mesh-elements on the drag, lift, and torque coefficients is shown in the Fig. 7. Although it is observed that there is an insignificant variation ($\approx 1\%$) of the coefficients with the change in the number of elements considered here, we have considered 120 elements on the ellipsoid to perform all the simulations reported

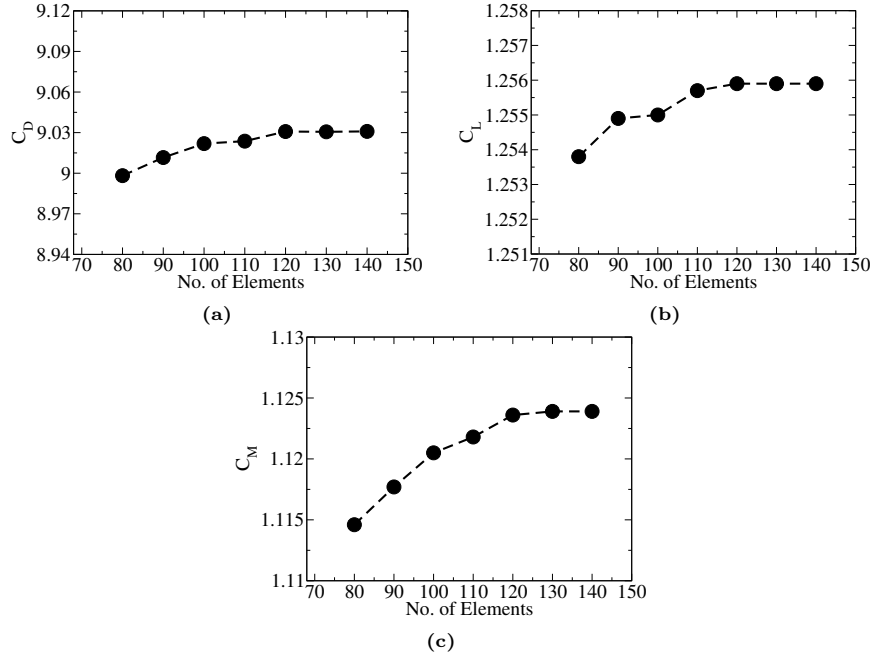


Fig. 7. Hydrodynamic coefficients variation with number of elements on ellipsoid surface at $Re_s = 10$ and $\theta = 0^\circ$

here.

3. Results and discussions

3.1. Flow structure around ellipsoid

The effects of shear Reynolds number Re_s and wall-normal distance along with orientation angle of the ellipsoid are shown with the roughness and particle induced disturbed flow field. There are significant contribution from the particle-wall separation distance and orientation of the particle to decide the flow characteristics around the ellipsoid. Fig. 8 shows streamlines across the ellipsoid at the plane of center (i.e. $y' = 0$), at $Re_s = 100$ for different value of wall-normal distances $\delta = 0.1, 0.5, 1.0, 1.5$ and orientation angle $\theta = 0^\circ, 45^\circ, 90^\circ$, and 135° . The streamline plots show that as the δ increases, the effect of wall diminishes rapidly. For $\delta > 0.5$, at all orientation angles, only the effect of ambient shear but not the wall roughness is observed. A similar observation is followed for all simulations carried out at lower Re_s 's (not shown here). Appearance of the wake behind the ellipsoid is mainly observed for higher values of Re_s 's. The structure of wake is also found to vary with separation from wall and the orientation angle. The location of the wake on either top (Fig. 8h) or bottom (Fig. 8p) part of the ellipsoid depends on the orientation angle to which

it is exposed to the background flow. In the case of $\theta = 90^\circ$, when a particle is away from the wall, the asymmetric wake is only due to ambient shear of flow.

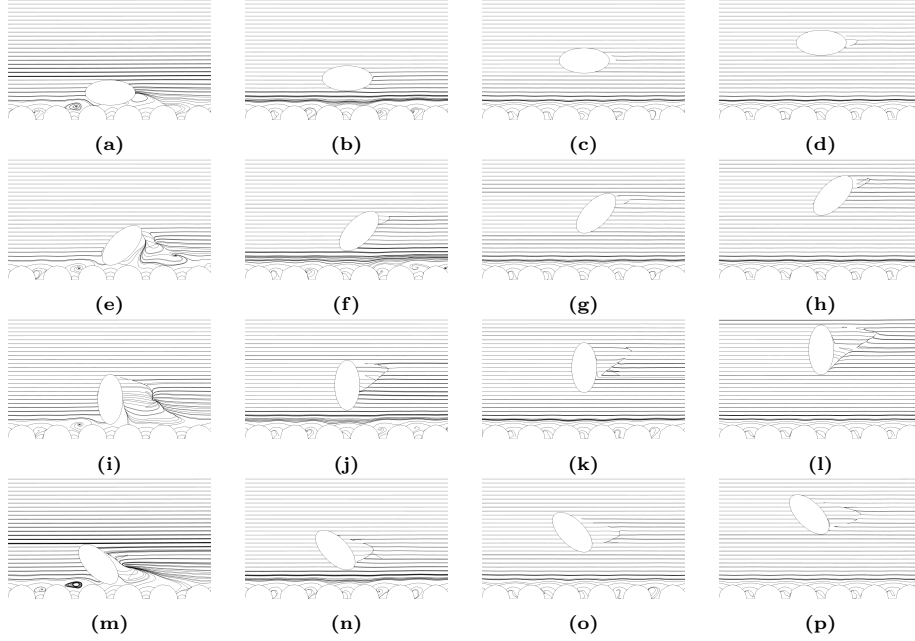


Fig. 8. Streamlines across particle at $Re_s = 100$, $\theta = 0^\circ$ (first row), 45° (second row), 90° (third row) and $\theta = 135^\circ$ (fourth row) and columns represents constant δ ($= 0.1, 0.5, 1.0, 1.5$) from left to right

The effect of Reynolds number on the development of wake behind the ellipsoid is visualised through the streamline plots Fig. 9. The figure shows the streamline plots for $\delta = 0.1$, $\theta = 45^\circ$, and at Re_s 10, 50, 100. For $\delta = 0.1$, the ellipsoid is sitting in the deepest cavity of rough wall. The flow between ellipsoid and wall is mainly due to channeling through the cavities on the rough wall. The accelerated flow observed in the gap for $\delta > 0.1$ is absent here, as ellipsoid acts as a barrier to the flow. Another important parameter is orientation angle which decides the location of the appearance of the recirculating zones. Fig. 9 shows that at lower Re_s , the flow is mostly streamlined over the ellipsoid, and a small recirculating zone is seen in the cavity of the rough wall. As Re_s increases (to 50), two counter-rotating vortices appear near the wall and flow separation happens at the bottom (near wall) part of the ellipsoid. Finally, for highest value of Re_s (i.e., 100) considered in the present study, the flow from bottom and top merges in the down stream and separation happens from the top of the ellipsoid. It is shown in Fig. 10 that at $\theta = 135^\circ$ the streamlines are completely different to those which are observed for $\theta = 45^\circ$. At $Re_s = 10$ (i.e. lowest value considered in study), a small vortex appear at upstream rather than downstream as in case of $\theta = 45^\circ$. Strength of circulation increases with increase in Re_s . Further, the detachment of boundary layer at high Re_s also

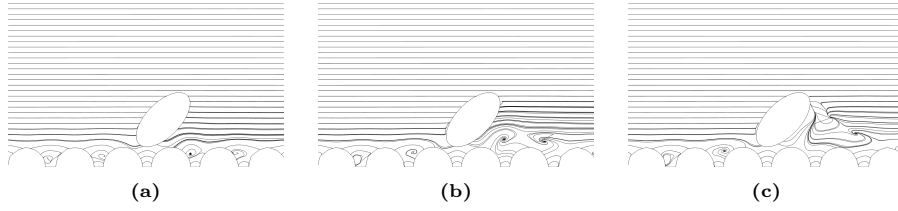


Fig. 9. Flow streamlines around the ellipsoid for $AR = 2$, $\theta = 45^\circ$, at (a) $Re_s = 10$ (b) $Re_s = 50$ (c) $Re_s = 100$

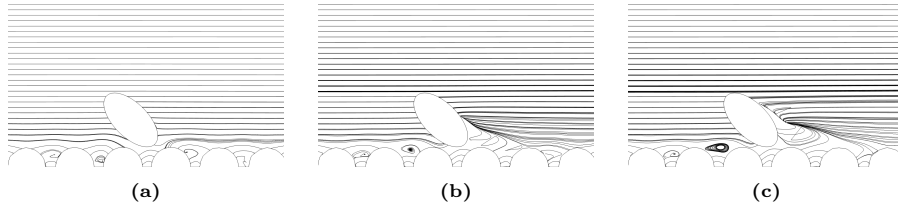


Fig. 10. Flow streamlines around the ellipsoid for $AR = 2$, $\theta = 135^\circ$, at (a) $Re_s = 10$ (b) $Re_s = 50$ (c) $Re_s = 100$

observed at lower half of ellipsoid, distinctly different from the case of 45° . This has significance in deciding the lift and torque acting on particle. As we will see in later sections, the lift and torque are found to change the direction based on detachment of the boundary layer, which in turn depends on orientation angle of the ellipsoid with the incident flow.

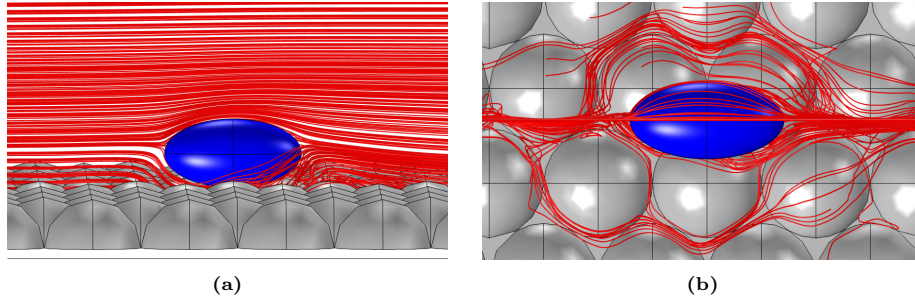


Fig. 11. 3D view of flow streamlines around the ellipsoid for $AR = 2$, $Re = 50$, $\theta = 0^\circ$, $\delta = 0.1$ from (a) side and (b) top view

In the above, all streamlines are shown in x-z 2D plane. A simultaneous 2-D view of the streamlines in x-z and x-y are shown for $\delta = 0.1d_p$ in at plane of particle center. Figs. 11a and 11b. The figures show the side and top view of 3D streamlines for $Re_s = 50$ and $\theta = 0^\circ$. As discussed earlier, the ellipsoid at this location acts as a barrier to flow. The channeling of flow through the rough cavity can be observed. Due to the roughness pattern on a surface and weak flow below ellipsoid, the recirculating vortices appear in deep cavities.

3.2. Drag coefficient

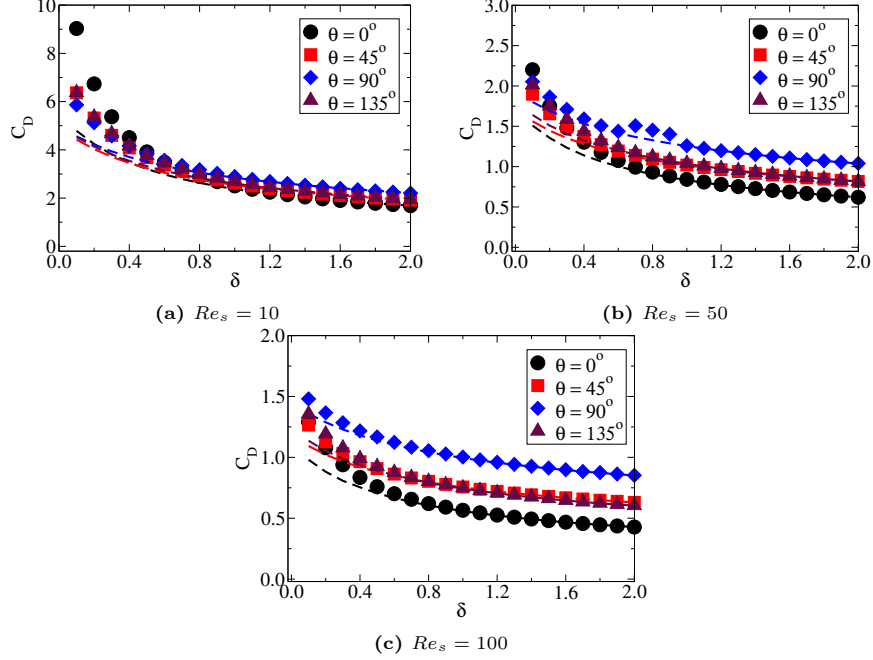


Fig. 12. Drag coefficient (C_D) as a function of wall normal distance δ at several Reynolds number. A dashed line with same color represent the corresponding values of C_D for smooth wall condition.

In this section, we present the drag coefficient as a function of wall-particle separation distance (δ) for different orientation angles (θ) and shear Reynolds numbers (Re_s), ranging between 10 and 100. In each of the cases, we have compared the results obtained for a rough wall with that of a smooth wall. Symbols with different shapes show C_D values obtained from the simulations with the rough wall, and dashed lines represent the C_D s for a smooth wall. For all Reynolds numbers, drag coefficients are much higher when the particle is placed near the wall (Fig. 12). There is a distinct difference in the effect of roughness on C_D at different Reynolds numbers. At low Re_s , if the particle is placed horizontally near the wall ($\delta < 0.5$), C_D for a rough wall is almost two times higher than that for the smooth wall. With an increase in wall-normal distance, the differences between two drag coefficients decrease for all the Reynolds numbers reported here. For $\delta > 1.0$, the effect of roughness becomes significant. Another notable observation at low Reynolds number is the significantly higher C_D values for horizontally aligned ellipsoid compared to the other orientation angles. This difference eventually vanishes at elevated shear Reynolds number. It is worth noting that for higher wall-particle gap ($\delta > 1.0$) drag coefficient in case of a vertically aligned particle is higher ($\approx 50\%$ for $Re_s = 100$) than the horizontal arrangement, even though the undisturbed velocity

interpolated at particle center is higher in case of the former. At low Reynolds number ($Re_s = 10$), the difference between drag coefficients for different angles of orientation decreases for the separation distance (δ) greater than 0.5. This observation motivates us to investigate the variation of drag coefficient as a function of angle of inclination with approaching fluid stream.

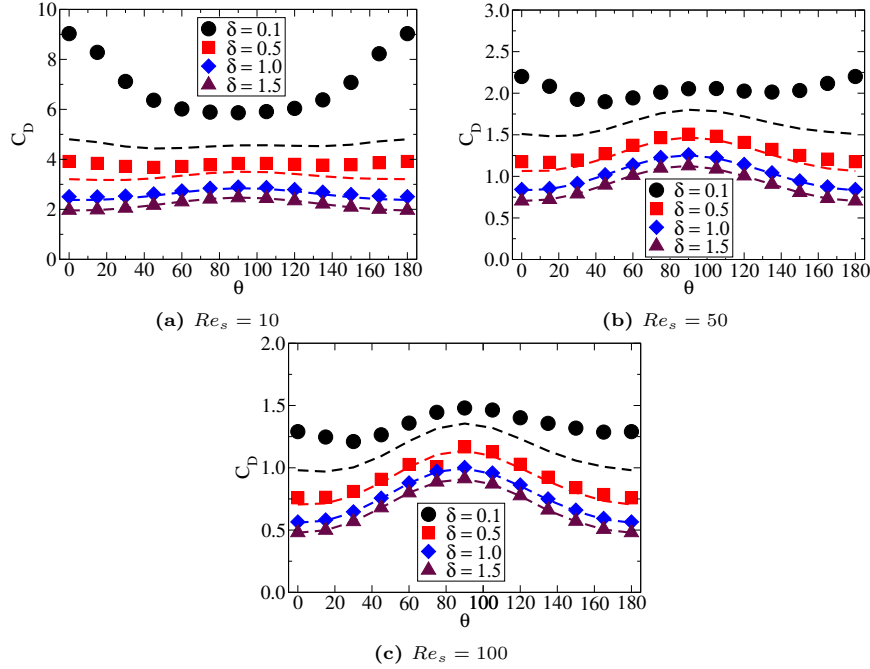


Fig. 13. Drag coefficient (C_D) as a function of orientation angle θ at several Reynolds number. A dashed line with same color represent the corresponding values of C_D for smooth wall condition.

The second important parametric effect to study is the orientation angle (θ) of the particle with the flow direction. Fig. 13 shows the variation of drag coefficient with θ for different wall particle separation distance distance (δ) and Reynolds number (Re_s). In the case of a smooth wall, the variation of C_D with θ at higher separation distance follows a similar trend reported by Happel and Brenner [33] for uniform flow over an ellipsoid particle. At low Reynolds number $Re_s = 10$, there is an insignificant variation of C_D with angle of inclination, but with increase in Reynolds number, C_D is maximum when $\theta = 90^\circ$. The effect of roughness becomes prominent when wall-particle separation (δ) is less than 0.5. At low shear Reynolds number ($Re_s = 10$), for the minimum separation distance reported here, drag coefficient is minimum when the particle is vertically aligned. For the horizontal alignment, the drag coefficient is almost 1.5 times higher than the vertical alignment. As shear Reynolds number increases, the above mentioned difference decreases. One important point to note here is that the undisturbed fluid velocity at the center of mass of the particle is higher in case of

a vertically aligned particle than that of a horizontally aligned one. To address this ambiguity, we have reported the variation of drag force as well besides drag coefficient, which is shown in Fig. 14.

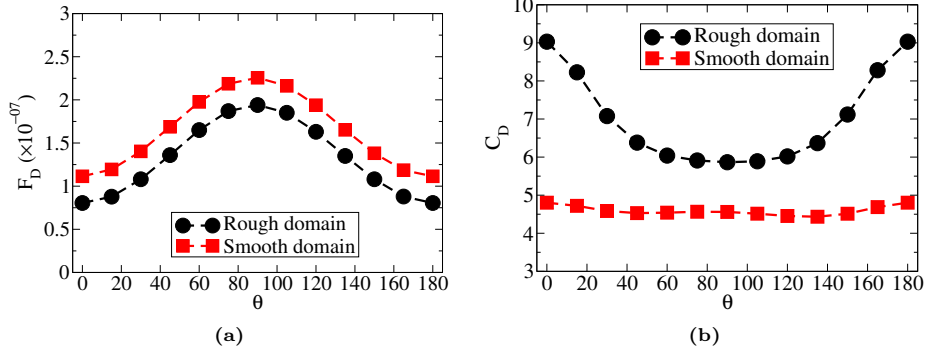


Fig. 14. Drag force F_D and drag Coefficient C_D as a function of θ for $Re_s = 10$ at $\delta = 0.1$

Fig. 13a shows that, away from the wall, there is a significant increase in the drag coefficient at $\theta = 90^\circ$. Similar to it, there is an increase in the undisturbed velocity, as mentioned earlier. To understand the contribution of viscous and pressure drag, we have computed these parameters separately and presented them in Fig. 15. We have restricted this exercise only for $\delta = 0.1$ and for two Reynolds numbers $Re_s = 10$ and 100. It is observed that at low Reynolds number, a viscous component of drag always dominates over the pressure drag for both the smooth and rough walls. Effect of wall roughness plays a more prominent role in case of the viscous drag for horizontally aligned particle. At high shear Reynolds number ($Re_s = 100$), the pressure drag coefficient is almost 1.5 times higher compared to the viscous counterpart for vertically aligned particle. This could be related to the formation of a wake in the rear end. One of the ob-

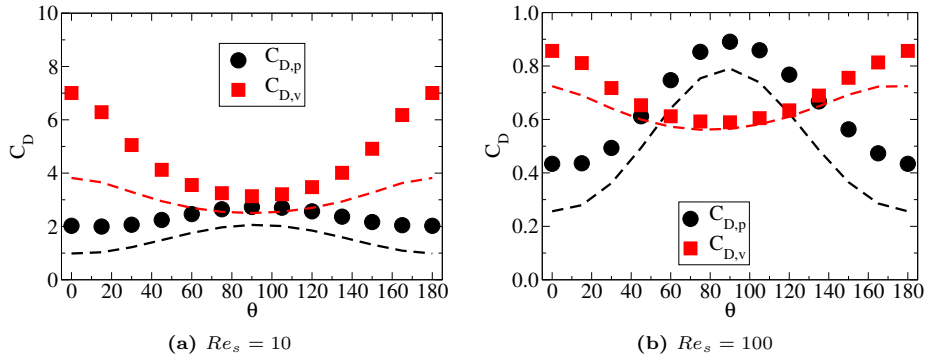


Fig. 15. Components of drop coefficient ($C_{d,p}$, $C_{d,v}$) as a function of orientation angle θ and, $\delta = 0.1$. A dashed line with same color represent the corresponding values of variable for smooth wall condition.

jectives of the present work is to express drag coefficient as a function of particle Reynolds number (Re_p), wall-normal distance, and angle of inclination of the major axis with the flow direction. It is to be noted that in the present work, main emphasis is given to the effect of wall roughness on the hydrodynamic force coefficient. Here, we have computed all the coefficients using only one aspect ratio. To include the effect of aspect ratio, we have used the shape factor k based upon theoretical formulation given in [34] and relevant modifications suggested by Ouchene et al. [26], which is applicable in the present scenario. It is observed from the simulations that the drag coefficients evolve as a function of $\sin(\theta)$ between angle $\theta = 0^\circ$ and 90° irrespective of the particle Reynolds numbers. Effect of particle Reynolds number is included in the drag coefficient of $\theta = 0^\circ$ and 90° . Effect of aspect ratio has also been included in the expression for drag coefficients for $\theta = 0^\circ$ and 90° [35, 26]. Separation distance from the wall (δ), one of the important parameters of major focus in the present study, is found to contribute non-linearly to the drag coefficient. A similar observation for the drag on a spherical particle has been reported by Zeng et al. [10] in an earlier study. With this described approach, the drag coefficient can be expressed by the following correlations.

$$C_D = C_{D,0} + (C_{D,90} - C_{D,0})\sin^2\theta \quad (9)$$

here,

$$C_{D,0} = \left(\frac{24}{Re_p}\right)(k_0\alpha_0 + \beta_0\omega^{-0.8}Re_p^{0.687} + \gamma_0(\omega - 1)^{0.63}Re_p^{0.41})$$

$$\alpha_0 = 1 + 0.001576\exp(2\delta) + \frac{3.895}{1.611(1 + 2\delta)}$$

$$\beta_0 = 0.15 - 0.03(1 + 2.03\delta)\exp(-0.392\delta)$$

$$\gamma_0 = 0.1497 - 0.01942(1 + 2.77\delta)\exp(-0.2921\delta)$$

and,

$$C_{D,90} = \left(\frac{24}{Re_p}\right)(k_{90}\alpha_{90} + \beta_{90}\omega^{-0.54}Re_p^{0.687} + \gamma_{90}\omega^{1.043}(\omega - 1)^{-0.17}Re_p^{0.41})$$

$$\alpha_{90} = 1 + 1.288\exp(0.05953\delta^{2.804}) + \frac{6.137}{6.479(1 + 0.05953\delta)}$$

$$\beta_{90} = 0.15 - 0.3824(1 + 2.599\delta)\exp(-0.344\delta)$$

$$\gamma_{90} = 0.2516 - 0.247(1 - 0.11\delta)\exp(\delta^{0.371})$$

Here, the shape factor k is presented by Ouchene et al. [26] as ,

$$k = k_0 = k_{90} = \frac{8}{3}\omega^{-1/3} \left[\frac{2\omega}{(\omega^2 - 1)} + \frac{2\omega^2 - 1}{(\omega^2 - 1)^{(3/2)}} \ln \frac{\omega + \sqrt{\omega^2 - 1}}{\omega - \sqrt{\omega^2 - 1}} \right]^{-1} \quad (10)$$

Above equation boils down to the correlation for the sphere reported by Schiller and Naumann [36] for $\omega = 1$ and $\delta \gg 1$. For $\omega = 1$ and in the limit of creeping flow and in the presence of a wall, the equation follows the correlation of Goldman et al. [37] for all δ , which was further simplified by Zeng et al. [10]. Accuracy of the present non-trivial correlation is evaluated by comparing it with the simulation results for a wide range of parameters. Fig. 16 shows comparison of drag coefficients obtained using correlation with that obtained from the simulations at two $Re_s = 10$ and 100 and for different orientation angles θ . In the figure, the drag coefficients have been reported as a function of separation distance from the wall (δ). It is observed from the figures that the prediction of the drag coefficients from the correlation matches well even for a very low separation distance $\delta < 0.5$ for both the shear-Reynolds numbers. The maximum deviation of about 8% between simulation and prediction by the correlation is observed at around $\delta \approx 1.0$ and $\theta = 0^\circ$ for all Re_s considered in study. Whereas, for other separation distances, the deviation does not exceed 3%. A similar trend is also observed for other orientation angles (Θ), considered in this study. At higher δ values, this deviation is reduced to 1%. The overall mean deviation for all simulated cases lies within 3.5%. Similarly, in Fig. 17, comparison of correlation prediction with simulation results is shown for C_D as function of θ at different δ . The figure shows that the correlation is fairly capable of producing accurate results from $\delta = 0.1$, where ellipsoid is placed very close to the wall to several particle diameters away from the wall. A

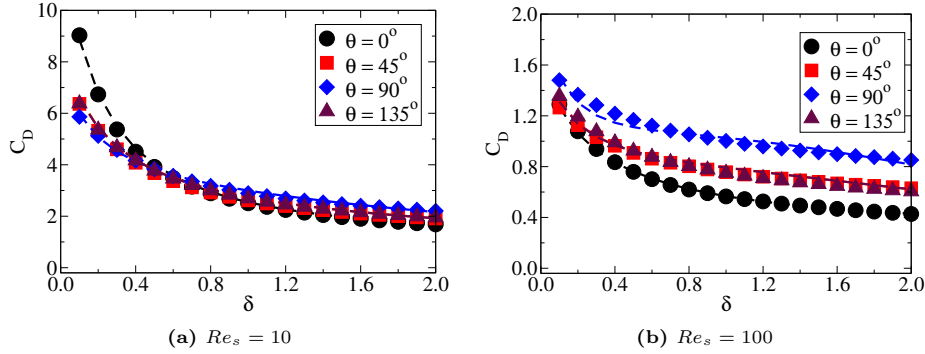


Fig. 16. C_D Vs δ for $Re_s = 10$ and 100 at different orientation angle (θ). The dashed line in corresponding color represents the fitted value from the correlation

goodness-of-fit between simulation results and correlation prediction is shown Fig. 18 for all shear Reynolds numbers, separation distances from the rough wall δ (0.1, 0.5, 1.0, and 2.0) and orientation angles θ ($0^\circ, 45^\circ, 90^\circ, 135^\circ$). The figure shows that all the data collapse along the diagonal line with a maximum error of 8%; confirms the applicability of the above correlation for calculating drag on an ellipsoidal particle near a rough wall.

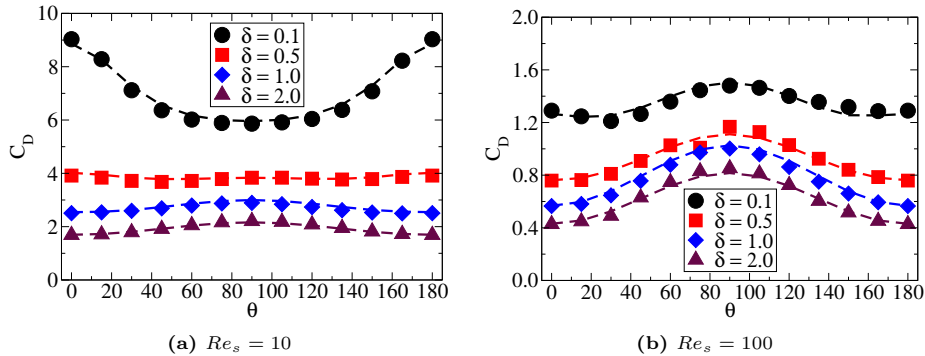


Fig. 17. C_D Vs θ for $Re_s = 10$ and 100 at different wall separation distance (δ). The dashed line in corresponding color represents the fitted value from the correlation

3.3. Lift coefficient

In this section, we report the lift coefficients for different particle-wall separation distances at three different shear-Reynolds numbers (Re_s). Fig. 19, shows the variation of lift coefficient (C_L) with δ at different inclination angles (0° to 135°). In addition to the results for rough wall, we have also presented the lift coefficients for a smooth wall. At lower shear-Reynolds number ($Re_s = 10$), the wall effects for both types of wall are very prominent below $\delta = 1.5$. At higher separation, the lift coefficient becomes almost independent of the separation distance. It is observed from the Fig. 19a that for all angles, the lift force act away from the wall but for $\theta = 45^\circ$. At this angle, a particle is effectively pushed towards the wall. Effect of rough wall is significant for a separation distance up to $\delta = 1.0$ at low shear-Reynolds number and up to $\delta = 0.5$ for higher shear Reynolds number as shown in Figs. 19b and 19c. For a horizontally aligned ellipsoid very near the wall, lift induced by a rough wall is almost 1.5 to 2 times higher than that exerted by a smooth wall across all the Reynolds numbers.

The variation of lift coefficients with inclination angle (θ) at different shear Reynolds numbers is presented in Fig. 20. Here, the angle is measured between the wall (or the direction of mean flow) and the major axis of the ellipsoid in a counter clock-wise direction. The lift coefficients show asymmetric nature at intermediate angles. It is shown in Fig. 20 that the roughness plays a crucial role in deciding the asymmetry in lift coefficient with change in angle at least when the particle is very close to the wall. It is also clear from the figures that with angle up to $\theta = 90^\circ$, the difference in lift coefficients between the smooth and rough wall is less than that for angles higher than $\theta = 90^\circ$. Another important observation is that the particle encounters a lift force towards the wall for an angle between 30° and 50° , which may be due to the creation of a low-pressure zone at the bottom rear end of the ellipsoid. An analysis of the contribution of viscous and pressure components towards the lift force provides more insight into that, which is discussed below.

The contribution from the pressure variation and viscous effect towards the

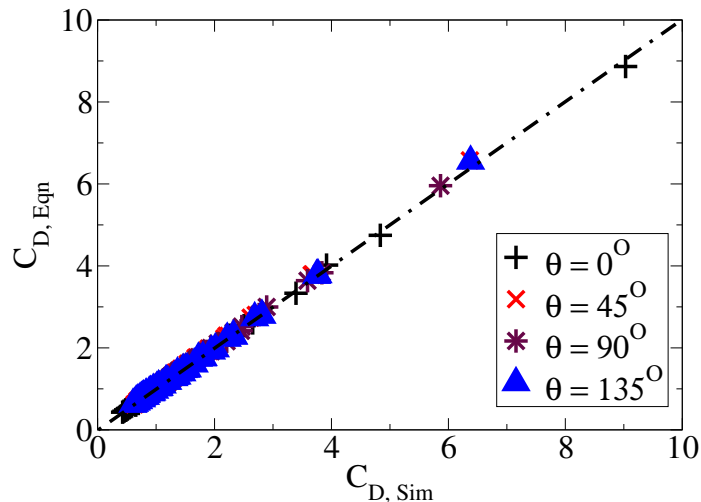


Fig. 18. Predicted C_D plotted against C_D from simulation data at various θ , and $(-\cdot-)$ represent line of $y = x$

total lift is depicted in Fig. 21. The figures show the variation of $C_{L,v}$ and $C_{L,p}$ Vs θ at $\delta = 0.1$ for $Re_s = 10$ and 100 . We have considered two different shear Reynolds numbers, $Re_s = 10$ and 100 , for this analysis. Results are shown for the case when a particle is placed very near the wall ($\delta = 0.1$). It is observed from the Fig. 21a that pressure contribution towards the total lift is much higher compared to its viscous counterpart even at low shear Reynolds number. Pressure lift works towards the wall up to an angle of 80° , but at a higher angle, net pressure force is exerted in the opposite direction. Maximum difference between the pressure to viscous contribution happens at an angle $\approx 150^\circ$; the ratio is about 6. A comparison with smooth wall at the lower shear Reynolds number (Fig. 21a) depicts that in the presence of a rough wall, both the viscous and pressure lift increases dramatically. The overall lift force acts away from the wall when a particle is very near the wall with an inclination angle of $> 120^\circ$. Such an observation has huge implications in the area of research that addresses the wall-deposition behaviour of nonspherical particles. It is shown in the figure that the pressure contribution to the lift for a smooth wall is much lower compared to the rough wall. The difference between those decreases at higher Reynolds number (Figs. 21a and 21b). Another important outcome of the present analysis is that in the presence of roughness, there is a significant increase in viscous lift away from the wall when the particle is aligned horizontally. Accepting the point that the scenario may change for the particle moves parallel to the wall, the present results can be a motivation for the wall modification to avoid particle deposition.

Turning our attention to develop the correlation for lift coefficient, we consider that the lift coefficient decreases exponentially with wall particle separation distance δ , magnitude of lift coefficient is a function of shear Reynolds number

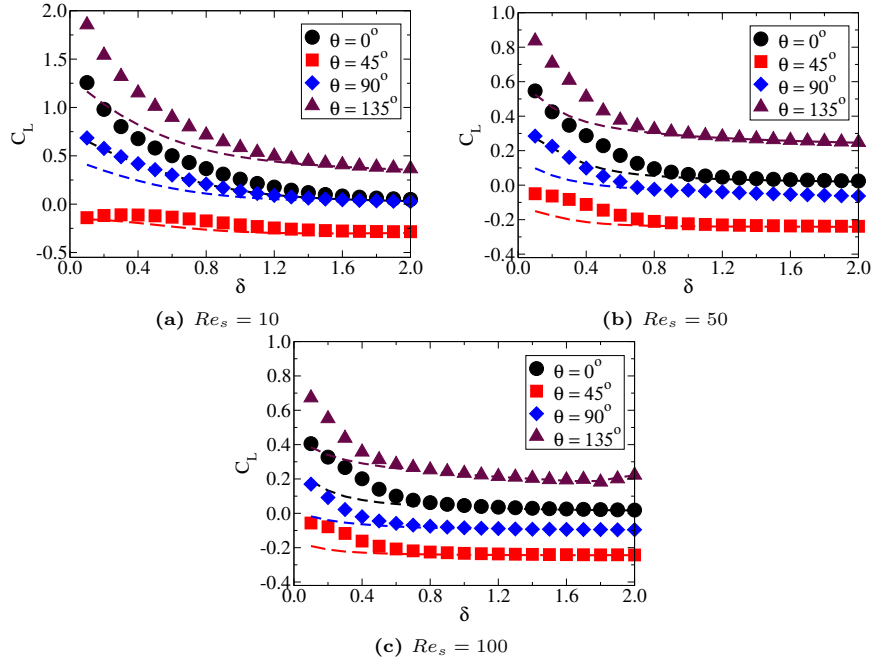


Fig. 19. Lift coefficient (C_L) as a function of wall normal distance δ at several Reynolds number. A dashed line with same color represent the corresponding values of C_L for smooth wall condition.

Re_s , which is related to particle Reynolds number Re_p as a function of δ , θ , and ω (aspect ratio of the ellipsoid). The effect of variation of angle is introduced through a skewed function of $\sin \theta \cos \theta$.

Using all the above criteria, we reach to the functional form of the correlation as,

$$C_L = C_{L,s} \{ \mathbf{f}(\delta, Re_s) + \mathbf{g}(\delta, Re_s) \sin[\mathbf{h}(\delta, Re_s)\theta] \cdot \cos[\mathbf{h}(\delta, Re_s)\theta] \} \quad (11)$$

Where, $C_{L,s}$ represents the lift for ellipsoidal particle resting on wall as reported earlier by Fillingham et al. [29].

$$C_{L,s} = \frac{3.663}{(\omega^{2.021} Re_p^2 + 0.1173\omega^{1.559})^{0.22}} \quad (12)$$

$\mathbf{f}(\delta, Re_s)$ takes care of the variation of lift coefficient including the change on direction of the lift.

$$\mathbf{f}(\delta, Re_s) = -0.043 - 0.00083Re_s + \frac{(0.93 + 0.0023Re_s)}{e^{(0.98\delta + 0.016Re_s\delta)}} \quad (13)$$

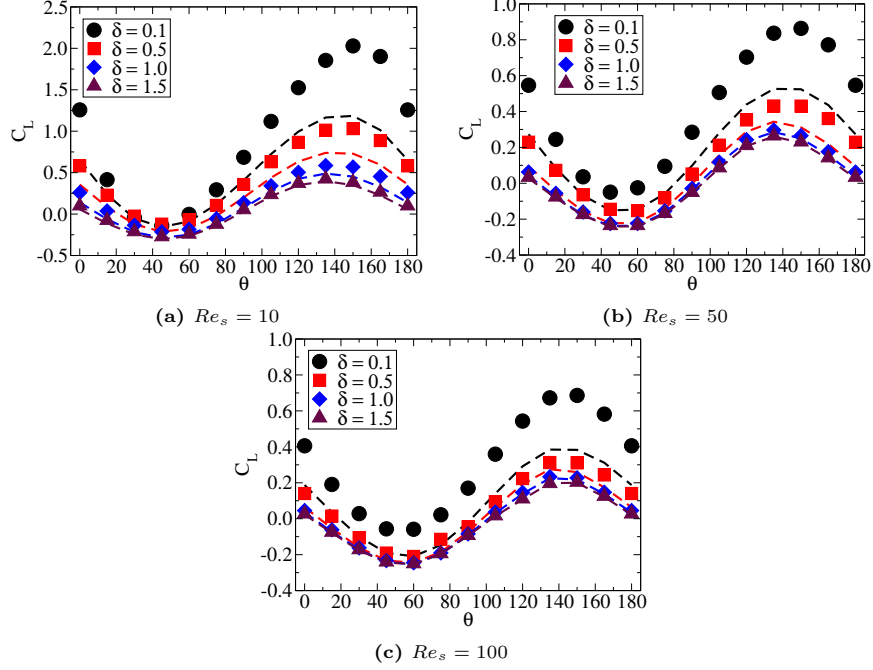


Fig. 20. Lift coefficient (C_L) as a function of orientation angle θ at several Reynolds number. A dashed line with same color represent the corresponding values of C_L for smooth wall condition.

$g(\delta, Re_s)$ is expressed as follows.

$$g(\delta, Re_s) = g'(\delta) + g''(\delta, Re_s) \quad (14)$$

Here, the first part is an exclusive function of δ , while the second part contains effect of variation of both the δ and Re_s .

$$g'(\delta) = 1.15e^{(-4.27\delta)} + 0.8e^{(0.17\delta)} \quad (15)$$

$$g''(\delta, Re_s) = -\left[0.285\delta + (0.001056Re_s\delta - 3.2)Re_s\right] \cdot e^{-(6.91 - \delta(0.16 - 0.0065Re_s))} \quad (16)$$

$h(\delta, Re_s)$ contributes to capture the skewed variation of C_L with θ .

$$h(\delta, Re_s) = 0.018Re_s + 0.96 \quad (17)$$

where Re_s is related to Re_p as,

$$Re_s = \frac{Re_p}{(0.3165 + \delta) + \frac{1}{2\sqrt{\omega}} + \frac{\sqrt{\omega}}{2}\left(1 - \frac{1}{\omega}\right)\sin^2\theta} \quad (18)$$

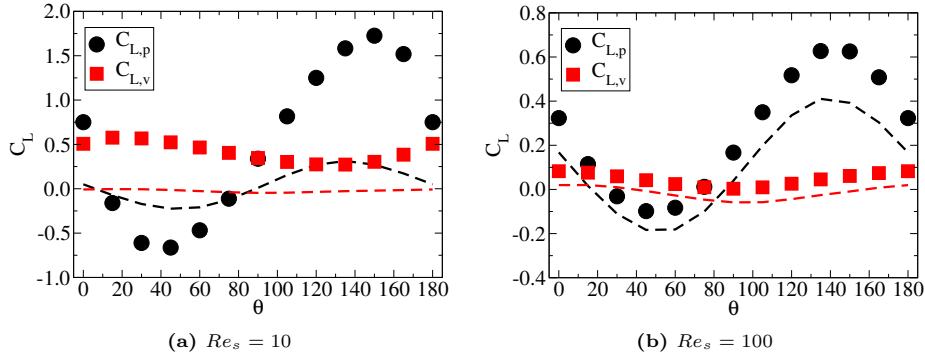


Fig. 21. components of lift coefficient ($C_{L,p}$, $C_{L,v}$) as a function of orientation angle θ and, $\delta = 0.1$. A dashed line with same color represent the corresponding values of variable for smooth wall condition.

Performance of the developed correlation in predicting the lift coefficient is assessed for different separation distance, angle of inclination, and for different Reynolds numbers. Fig. 22 shows the comparison between lift coefficient calculated using simulations and that predicted from the correlation as function of δ at $Re_s = 10$ (Fig. 22a) and $Re_s = 100$ (Fig. 22b). It is observed that the predictions from the correlation match well with the simulations results in majority of the cases. At $Re_s = 10$, when the particle is placed very near the wall at an 45° , a correlation over-predicts the lift coefficient. In case of $Re_s = 100$, at angle 90° , correlation over-predicts the lift coefficients for all the separation distances (Fig. 22b). However, the expression can successfully reports the trends of lift variation with wall separation distance at all shear Reynolds numbers.

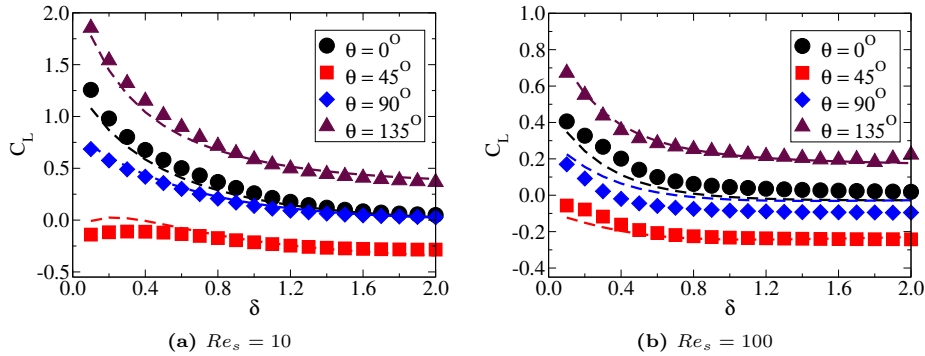


Fig. 22. C_L Vs δ for $Re_s = 10$ and 100 at different orientation angle (θ). The dashed line in corresponding color represents the fitted value from the correlation

Lift coefficients calculated from simulation and predicted by correlation are plotted as function of θ at several wall separation distance δ , as shown in Fig. 23. A good agreement is observed for both the shear-Reynolds numbers. Most importantly, the asymmetry that occurs at a lower separation distance is well

captured by the correlation. It is observed that, at high shear-Reynolds number ($Re_s = 100$) when the wall separation distance (δ) is 0.5, correlation under-predicts the lift coefficients. To obtain a comprehensive assessment of the performance of correlation, developed in the present study, we have plotted the lift coefficient predicted by correlation with that obtained from simulations for $\delta = 0.1, 0.5, 1.0,$ and $2.0,$ and $\theta = 0^\circ, 45^\circ, 90^\circ,$ and 135° in Fig. 24. Even though majority of the data collapses along a diagonal line in Fig. 24, there is significant deviation when the lift coefficient is less than 0.1. At a lower shear Reynolds number, the proposed correlation can predict the simulated results fairly well with a maximum deviation of 20% for all the orientation angles but for $\theta = 0^\circ$. The error is maximum at those points where there is a change in direction of the lift forces. At a higher shear Reynolds number the lift becomes comparatively small and changes its direction as the particle moves away from the wall at a particular orientation angle. The region (wall separation distance) where lift is significantly small ($O(10^{-2})$) and changes sign, the proposed equation gives a large error as shown in the inset of Fig. 24.

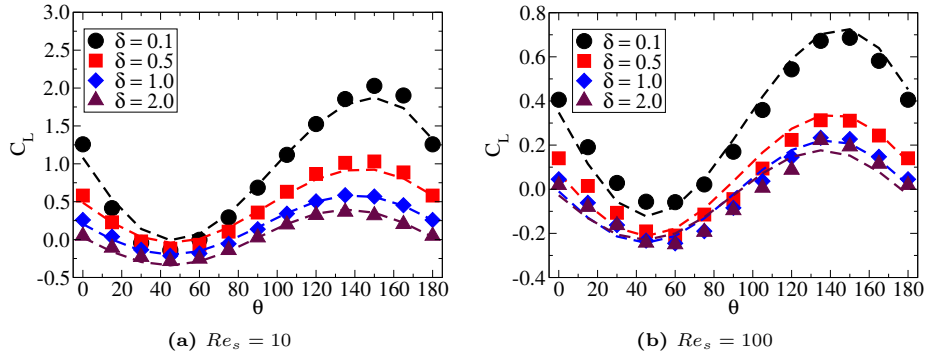


Fig. 23. C_L Vs θ for $Re_s = 10$ and 100 at different wall separation distance (δ). The dashed line in corresponding color represents the fitted value from the correlation

3.4. Torque coefficient

For a nonspherical particle immersed in a shear flow, besides calculating drag and lift, it is also essential to get an estimate of the torque. This section analyses the torque coefficient around its center of mass point for three different shear Reynolds numbers, different angles of orientation, and wall separation distances. We compare the results for both the rough and smooth walls. Fig. 25 shows a variation of torque coefficient C_M with wall-normal distance δ for four different orientation angles (θ) and at different Reynolds numbers. We use the right-hand coordinate system to express the direction of torque. Legends used in the figures have same significances that have been stated earlier. It is observed in the figure that C_M decreases exponentially as ellipsoid moves away from the wall, a similar trend for the drag and lift coefficients.

At the lower shear Reynolds number, reported here ($Re_s = 10$) torque coefficient (C_M) is positive even for horizontally aligned particle placed near the

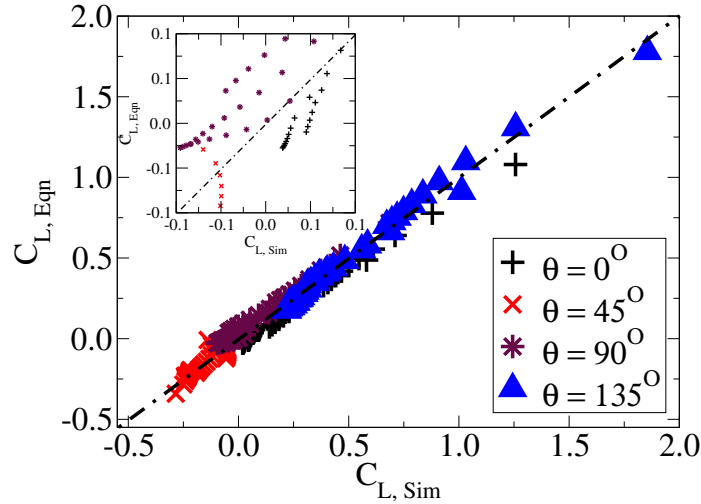


Fig. 24. Predicted C_L plotted against C_D from simulation data at various θ , and $(- \cdot -)$ represent line of $y = x$

wall. For an angle of inclination 0° , change in torque coefficient is observed up to wall separation distance, $\delta \approx 1$. With an increase in Reynolds number, the distance of influence decreases gradually. In case of $Re_s = 50$ (Fig. 25b), the δ after which C_M does not show any variation is $\delta \approx 0.7$, whereas for $Re_s = 100$ that is $\delta < 0.5$ (Fig. 25c). A similar trend is observed for other angles as well. The figures illustrate that there is a three to five-fold decrease in torque coefficient for a ten times increase in Reynolds number for minimum wall separation distance.

Fig. 26 show the variation of torque coefficient for different inclination angles and at three different shear Reynolds numbers. It is to be noted that the angle is changed in the plane of shear. It is shown in the Fig. 26a that the rough wall has very prominent effect for the lowest wall-separation distance ($\delta = 0.1$). With an increase in the distance from the wall, influence of the nature of the wall becomes insignificant. Extent of asymmetry in C_M increases with increase in Shear Reynolds number (Fig. 26). At shear-Reynolds numbers, $Re_s = 50$ and 100, if the particle-wall separation distance is ≥ 0.5 , torque on the particle acts in the negative direction when the inclination angle is between $> 0^\circ$ and 80° (Figs. 26b and 26c).

4. Conclusion

Particle-laden flows with anisotropic particles find applications in industrial and natural processes. The interactions between anisotropic particles with fluid flow are complex in nature because the orientation of particles changes the fluid flow behaviour. Presence of an uneven wall in the vicinity of the particle adds additional complexity. Earlier efforts were reported to estimate the forces in

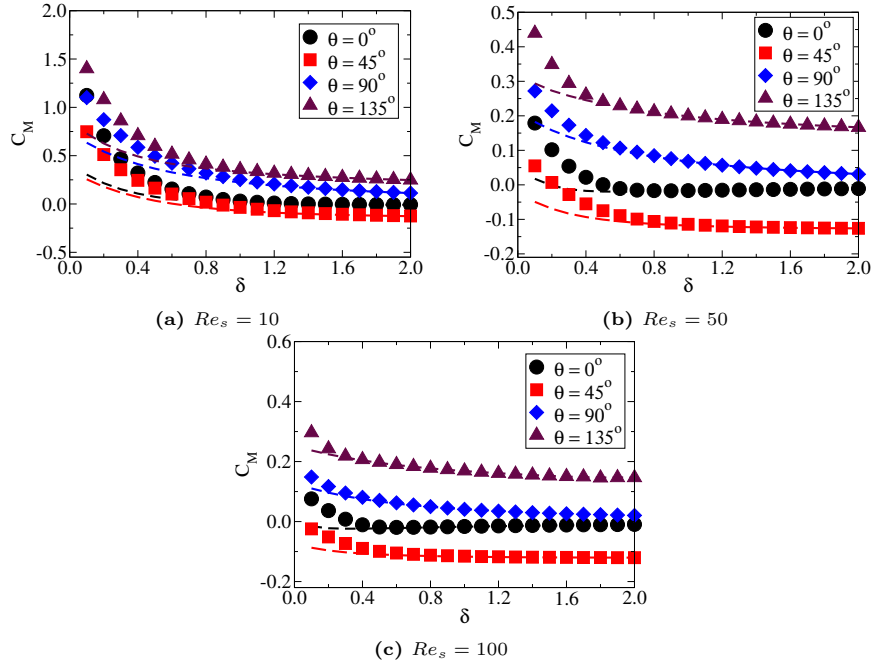


Fig. 25. Torque coefficient (C_m) as a function of wall normal distance δ at several Reynolds number. A dashed line with same color represent the corresponding values of C_m for smooth wall condition.

the presence of rough wall but for spherical particles only. We have performed numerical simulations (with high spatial resolution) to estimate the forces on an ellipsoidal particle placed in the vicinity of a rough wall at different wall separation distances and inclination angles. To create the wall roughness, we have followed the approach already demonstrated by Lee and Balachandar [8]. Simulations have been performed for a range of Reynolds numbers Re_s ($10 \leq Re_s \leq 100$), δ ($0.1 \leq \delta \leq 2$), and θ ($0^\circ \leq \theta \leq 180^\circ$). Undisturbed (by the ellipsoidal) fluid velocity at particle center of mass location is obtained using an empty channel simulation with wall roughness only. This velocity is used to calculate the drag, lift, and torque coefficients. Simulations with a smooth wall for the similar flow conditions have also been performed and compared to quantify the effect of wall roughness.

Streamline plots over the ellipsoid qualitatively depicts the appearance of the flow separation and recirculating zone at the top edge for $\theta < 90$ and at the bottom edge for $\theta > 90$. Such a flow separation plays an essential role in deciding the direction of the lift force on the particle. If the particle is placed near the wall at low shear Reynolds number, C_d is almost two times higher than the smooth wall. The effect of a wall-roughness becomes insignificant away from the wall ($\delta > 1.0$). The drag coefficient for a vertically placed particle at a higher Reynolds number ($Re_s \approx 100$) is larger than the horizontally placed particle,

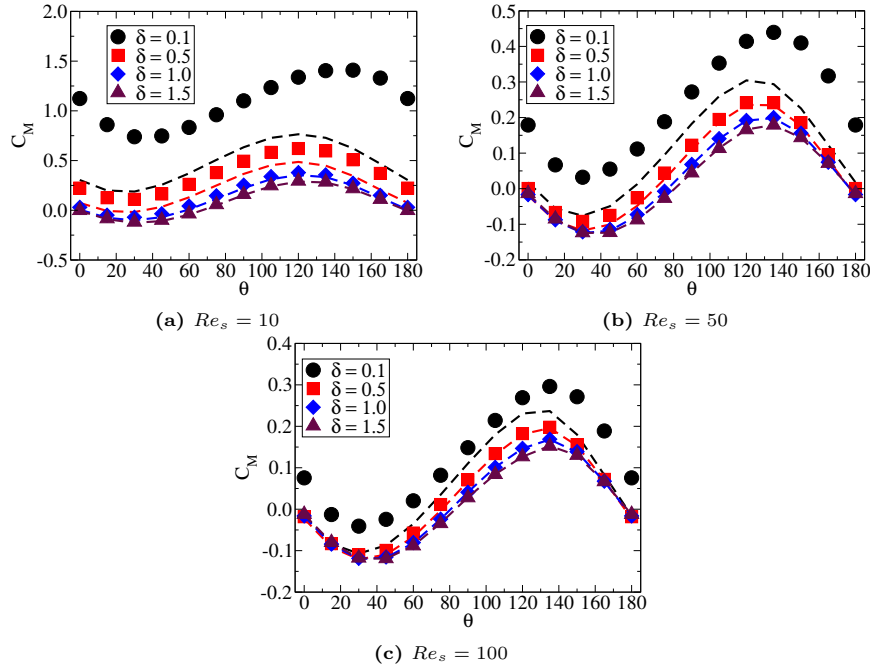


Fig. 26. Torque coefficient (C_m) as a function of orientation angle θ at several Reynolds number. A dashed line with same colour represent the corresponding values of C_m for smooth wall condition.

even though a higher undisturbed velocity occurs at the particle location. At low Re , when the particle is placed very near the wall, a viscous component of the drag dominates over the pressure component for both types of wall. If the particle is vertically aligned at a higher Reynolds number, the pressure drag is almost 1.5 times higher than the viscous counterpart. In case of lift coefficient, the effect of nature of wall is prominent below separation distance, $\delta = 1.5$. In all the cases, lift acts away from the wall except the angle between 30° to 50° . Effect of the rough wall is prominent up to a separation distance (δ) of 1.0. Irrespective of the nature of the wall, an asymmetry is observed in the variation of lift coefficient as a function of an angle of the particle's major axis with the wall. At low wall separation distance, the asymmetry is augmented by the wall roughness.

From the analysis of forces on the ellipsoidal particles, we develop and present the semi-empirical correlations for the drag and lift coefficients for different wall separation distances (including roughness) and different inclination angles. The correlations are applicable for particle Reynolds numbers up to 250. The accuracies of these correlations are verified by comparing predictions by the correlations with the simulation results for a wide range of parameters. Maximum relative deviation for drag coefficient is found to be 8%. However, correlation of the lift suffers from the accuracy at lower values of lift coefficients when there

is a change in direction of the lift.

One of the important limitations of the present study is that the simulations have been performed for a single aspect ratio. Therefore, the developed correlations are to be justified through further studies using ellipsoid with other aspect ratios. The second important limitation is that the effect of roughness has been demonstrated only for a single roughness pattern. A detailed study to establish the effect of different roughness patterns will be an interesting future scope.

Acknowledgement

This work is supported by IRCC IIT Bombay (No: RD/0512-IRCCSH0-017).

References

References

1. Kruggel-Emden H, Vollmari K. Flow-regime transitions in fluidized beds of non-spherical particles. *Particuology* 2016;29:1–15. doi:<https://doi.org/10.1016/j.partic.2016.01.004>.
2. Mills D. Pneumatic conveying design guide. Elsevier; 2003.
3. Kleinstreuer C, Feng Y. Computational analysis of non-spherical particle transport and deposition in shear flow with application to lung aerosol dynamics—a review. *Journal of Biomechanical Engineering* 2013;135(2). doi:10.1115/1.4023236.
4. Tadros TF. Rheology of dispersions: principles and applications. John Wiley & Sons; 2011.
5. Ogawa K, Yoshikawa S, Suguro A, Ikeda J, Ogawa H. Flow characteristics and circular pipe flow of pulp-suspension. *Journal of Chemical Engineering of Japan* 1990;23(1):1–6. doi:10.1252/jcej.23.1.
6. Lundell F, Söderberg L, Alfredsson P. Fluid mechanics of papermaking. *Annual Review of Fluid Mechanics* 2011;43:195–217. doi:10.1146/annurev-fluid-122109-160700.
7. Cui H, Grace JR. Flow of pulp fibre suspension and slurries: A review. *International Journal of Multiphase Flow* 2007;33(9):921–34. doi:<https://doi.org/10.1016/j.ijmultiphaseflow.2007.03.004>.
8. Lee H, Balachandar S. Effects of wall roughness on drag and lift forces of a particle at finite reynolds number. *International Journal of Multiphase Flow* 2017;88:116–32. doi:10.1016/j.ijmultiphaseflow.2016.09.006.
9. Zeng L, Balachandar S, Fischer P. Wall-induced forces on a rigid sphere at finite reynolds number. *Journal of Fluid Mechanics* 2005;536:1–25. doi:10.1017/S0022112005004738.

10. Zeng L, Najjar F, Balachandar S, Fischer P. Forces on finite-sized particle located close to a wall in a linear shear flow. *Physics of Fluids* 2009;21:033302. doi:10.1063/1.3082232.
11. Jeffery GB, Filon LNG. The motion of ellipsoidal particles immersed in a viscous fluid. *Proceedings of the Royal Society of London Series A, Containing Papers of a Mathematical and Physical Character* 1922;102(715):161–79. doi:10.1098/rspa.1922.0078.
12. Brenner H. The stokes resistance of an arbitrary particle. *Chemical Engineering Science* 1963;18(1):1–25. doi:10.1016/0009-2509(63)80001-9.
13. Brenner H. The stokes resistance of an arbitrary particle—ii: An extension. *Chemical Engineering Science* 1964;19(9):599–629. doi:https://doi.org/10.1016/0009-2509(64)85051-X.
14. Brenner H. The stokes resistance of an arbitrary particle—iii: Shear fields. *Chemical Engineering Science* 1964;19(9):631–51. doi:https://doi.org/10.1016/0009-2509(64)85052-1.
15. Harper EY, Chang ID. Maximum dissipation resulting from lift in a slow viscous shear flow. *Journal of Fluid Mechanics* 1968;33(2):209–25. doi:10.1017/S0022112068001254.
16. Lin J, Shi X, Yu Z. The motion of fibers in an evolving mixing layer. *International Journal of Multiphase Flow* 2003;29(8):1355–72. doi:https://doi.org/10.1016/S0301-9322(03)00086-7.
17. Gavze E, Shapiro M. Particles in a shear flow near a solid wall: Effect of nonsphericity on forces and velocities. *International Journal of Multiphase Flow* 1997;23(1):155–82. doi:https://doi.org/10.1016/S0301-9322(96)00054-7.
18. Pozrikidis C. Orbiting motion of a freely suspended spheroid near a plane wall. *Journal of Fluid Mechanics* 2005;541:105–14. doi:10.1017/S0022112005006117.
19. Lee SY, Hyun JY. Analysis of forces acting on the non-spherical particle near a wall. 2015. doi:https://doi.org/10.1007/s13534-015-0205-z.
20. Kim DK, Hyun JY, Kim SC, Kim HS, Lee SY. Inertial effects on cylindrical particle migration in linear shear flow near a wall. *Microfluidics and Nanofluidics* 2016;20(5):75. doi:https://doi.org/10.1007/s10404-016-1742-1.
21. Smith FT. Free motion of a body in a boundary layer or channel flow. *Journal of Fluid Mechanics* 2017;813:279–300. doi:10.1017/jfm.2016.706.
22. Zarghami A, Padding J. Drag, lift and torque acting on a two-dimensional non-spherical particle near a wall. *Advanced Powder Technology* 2018;29:1507–17. doi:10.1016/j.apt.2018.03.019.

23. Palmer RA, Smith FT. When a small thin two-dimensional body enters a viscous wall layer. *European Journal of Applied Mathematics* 2020;31(6):1002–28. doi:10.1017/S0956792519000378.
24. Holzer A, Sommerfeld M. New simple correlation formula for the drag coefficient of non-spherical particles. *Powder Technology* 2008;184(3):361–5. doi:https://doi.org/10.1016/j.powtec.2007.08.021.
25. Zastawny M, Mallouppas G, Zhao F, Wachem BV. Derivation of drag and lift forces and torque coefficients for non-spherical particles in flows. *International Journal of Multiphase Flow* 2012;39:227–39. doi:10.1016/j.ijmultiphaseflow.2011.09.004.
26. Ouchene R, Khalij M, Arcen B, Tanière A. A new set of correlations of drag, lift and torque coefficients for non-spherical particles and large reynolds numbers. *Powder Technology* 2016;303:33 – 43. doi:10.1016/j.powtec.2016.07.067.
27. Sanjeevi SK, Kuipers J, Padding JT. Drag, lift and torque correlations for non-spherical particles from stokes limit to high reynolds numbers. *International Journal of Multiphase Flow* 2018;106:325–37. doi:10.1016/j.ijmultiphaseflow.2018.05.011.
28. Frohlich K, Meinke M, Schröder W. Correlations for inclined prolates based on highly resolved simulations. *Journal of Fluid Mechanics* 2020;901:A5. doi:10.1017/jfm.2020.482.
29. Fillingham P, Vaddi RS, Bruning A, Israel G, Novosselov IV. Drag, lift, and torque on a prolate spheroid resting on a smooth surface in a linear shear flow. *Powder Technology* 2021;377:958–65. doi:https://doi.org/10.1016/j.powtec.2020.09.042.
30. Andersson HI, Jiang F. Forces and torques on a prolate spheroid: low-reynolds-number and attack angle effects. *Acta Mechanica* 2019;230(2). doi:10.1007/s00707-018-2325-x.
31. Ouchene R, Khalij M, Taniere A, Arcen B. Drag, lift and torque coefficients for ellipsoidal particles: from low to moderate particle reynolds numbers. *Computers and Fluids* 2015;113:53–64. doi:10.1016/j.compfluid.2014.12.005.
32. Sanjeevi SKP, Padding JT. On the orientational dependence of drag experienced by spheroids. *Journal of Fluid Mechanics* 2017;820:R1. doi:10.1017/jfm.2017.239.
33. Happel J, Brenner H. Low Reynolds Number Hydrodynamics with Special Applications to Particulate Media. Springer Netherlands (Martinus Nijhoff Publishers, The Hague); 1983. doi:https://doi.org/10.1007/978-94-009-8352-6.

34. Lamb H. Hydrodynamics. Cambridge university press; 1993.
35. Loth E. Drag of non-spherical solid particles of regular and irregular shape. *Powder Technology* 2008;182(3):342–53. doi:<https://doi.org/10.1016/j.powtec.2007.06.001>.
36. Schiller L, Naumann A. Fundamental calculations in gravitational processing. *Zeitschrift Des Vereines Deutscher Ingenieure* 1933;77:318–20.
37. Goldman A, Cox R, Brenner H. Slow viscous motion of a sphere parallel to a plane wall—ii couette flow. *Chemical Engineering Science* 1967;22(4):653–60. doi:[https://doi.org/10.1016/0009-2509\(67\)80048-4](https://doi.org/10.1016/0009-2509(67)80048-4).